

k -dependent spectrum and optical conductivity near metal-insulator transition in multi-orbital Hubbard bands

Oki Miura and Takeo Fujiwara

Department of Applied Physics, University of Tokyo, Bunkyo-ku, Tokyo 113-8656, Japan

We apply the dynamical mean field theory (DMFT) in the iterative perturbation theory (IPT) to doubly degenerate e_g bands and triply degenerate t_{2g} bands on a simple cubic lattice and calculate the spectrum and optical conductivity in arbitrary electron occupation. The spectrum simultaneously shows the effects of multiplet structure and DMFT together with the electron ionization and affinity levels of different electron occupations, coherent peaks at the Fermi energy in the metallic phase and a gap at an integer filling of electrons for sufficiently large Coulomb U . We also calculate the critical value of the Coulomb U for degenerate orbitals.

PACS numbers:

I. INTRODUCTION

Many physical properties in strongly correlated systems have been studied extensively both experimentally and theoretically. These are not well described, however, by the local density approximation (LDA) based on the density functional theory (DFT). LDA+ U method has been developed beyond LDA, [1] and it works reasonably well for the insulating case near metal-insulator transition in strongly correlated systems. However, low-energy excitations in metallic phase near metal-insulator transition can not be treated by LDA+ U method and more sophisticated approaches are needed.

Recently the dynamical mean field theory (DMFT) has been developed and applied to some model systems, which led us to a unified picture of both low- and high-energy excitations in the anomalous metallic phase near metal-insulator transition. [2] DMFT is based on the mapping of many body systems in bulk onto a single impurity problem, where the off-site Coulomb interaction can be neglected, subject to a self-consistency condition. The combination of DMFT with LDA is applicable to discuss realistic systems. [3, 4] The combination of DMFT with the GW approximation has been developed to include the off-site Coulomb interaction. [5]

To solve the mapped single impurity problem within DMFT, one can use several computational schemes such as the quantum Monte Carlo method (QMC), [6, 7] the iterative perturbation theory (IPT), [8, 9] the non-crossing approximation (NCA) [10] and the exact diagonalization (ED). [11] While QMC is not applicable in the low temperature limit, ED yields only a discrete number of poles for the density of states. Moreover, the exact calculations such as QMC and ED can only be suitable for simple model Hamiltonians. To carry out realistic calculations in realistic materials, the approximate ones such as IPT or NCA would be more suitable due to its CPU-time, though IPT is not applicable for cases of large Coulomb interactions and NCA can not yield the Fermi liquid behavior at low energies and in low temperature limit. [12]

The aim of the present paper is to apply the general-

ized DMFT-IPT method for multi-bands on lattices [9] to the doubly degenerate e_g bands and the triply degenerate t_{2g} bands on a simple cubic lattice and discuss the k -dependent spectra, the local Green's function and the optical conductivity near metal-insulator transition. In Sec. II we will give the general formulation of the dynamical mean field theory and the optical conductivity. In Sec. III we will show our numerical results such as k -dependent spectrum, the imaginary part of the local Green's function and the optical conductivity for both $n = 0.5$ and $n < 0.5$ cases. Finally we summarize our results in Sec. IV.

II. FORMULATION

A. Hamiltonian

We proceed with the Hubbard-type Hamiltonian:

$$H = \sum_{jm\sigma} \epsilon_d^0 c_{jm\sigma}^\dagger c_{jm\sigma} + \sum_{jj'\sigma mm'} h_{mm'\sigma}^{jj'} c_{jm\sigma}^\dagger c_{j'm'\sigma} + U \sum_{jmm'} n_{jm\uparrow} n_{jm'\downarrow} + U \sum_{j\sigma m > m'} n_{jm\sigma} n_{jm'\sigma}. \quad (1)$$

The first and second terms are the single-particle tight-binding Hamiltonian. Note that index j in the sum of Eq. (1) is running for correlated sites, $\{m\}$ for orbital indices and $\{\sigma\}$ for spins. U is the on-site Coulomb interaction and the exchange interaction is neglected here.

B. Dynamical mean field theory

Lattice Green's function and local Green's function are defined as

$$G_{m\sigma m'\sigma'}(\mathbf{k}, i\omega_n) = [(i\omega_n + \mu - \epsilon_d^0) \mathbf{1} - h(\mathbf{k}) - \Sigma(i\omega_n)]_{m\sigma m'\sigma'}^{-1}, \quad (2)$$

$$G_{m\sigma m'\sigma'}(i\omega_n) = \frac{1}{V} \int d\mathbf{k} G_{m\sigma m'\sigma'}(\mathbf{k}, i\omega_n), \quad (3)$$

where $h(\mathbf{k})$, μ and $\mathbf{1}$ are the single-particle part of the Hamiltonian in \mathbf{k} -space, the chemical potential and the unit matrix. Here we neglect the \mathbf{k} -dependence of the self-energy Σ within the framework of DMFT. The chemical potential μ is determined to satisfy the Luttinger's theorem. [14]

The IPT method was developed by Kajueter and Kotliar for non-degenerate orbital [8] and generalized by Fujiwara et al. for multi-orbital bands [9] on arbitrary electron occupation. In the IPT scheme, we assume the self-energy as

$$\Sigma(i\omega_n) = Un(N_{\text{deg}} - 1) + \frac{A\Sigma^{(2)}(i\omega_n)}{1 - B(i\omega_n)\Sigma^{(2)}(i\omega_n)}, \quad (4)$$

where $\Sigma^{(2)}(i\omega_n)$ is the second-order self-energy, $n_d = \sum_{m\sigma} n_{jm\sigma} = nN_{\text{deg}}$ is the total d-electron occupation number, n is the occupation number per each orbital and N_{deg} is the degree of the degeneracy with respect to spins and orbitals. The coefficients A and $B(i\omega_n)$ are determined by requiring the self-energy $\Sigma(i\omega_n)$ to be exact in the high-frequency limit ($i\omega_n \rightarrow \infty$), and in the atomic limit ($U \rightarrow \infty$) [9]. $\Sigma^{(2)}(i\omega_n)$ is explicitly proportional to $(N_{\text{deg}} - 1)$ and U^2 .

The local Green's function is calculated in a form

$$G_{mm'}(i\omega_n) = \frac{1}{V} \sum_{\alpha} \int d\mathbf{k} U_{m\alpha}(\mathbf{k}) G_{\alpha}(\mathbf{k}, i\omega_n) U_{\alpha m'}^{-1}(\mathbf{k}), \quad (5)$$

$$G_{\alpha}(\mathbf{k}, i\omega_n) = \frac{1}{i\omega_n + \mu - \epsilon_d^0 - \epsilon_{\alpha}(\mathbf{k}) - \Sigma(i\omega_n)}, \quad (6)$$

where the Hamiltonian matrix $h(\mathbf{k})$ is diagonalized to be $\epsilon_{\alpha}(\mathbf{k})$ by the unitary matrix $U(\mathbf{k})$. The \mathbf{k} -integration is carried out by using a generalized tetrahedron method. [9] The 8×243 \mathbf{k} -points are used in the \mathbf{k} -integration within the whole Brillouin zone. For a paramagnetic and orbital degenerate system, the local Green's function becomes diagonal after the \mathbf{k} -integration. The Padé approximation is adopted for analytic continuation of the Green's function from the Matsubara frequencies $i\omega_n$ to the real ω -axis.

C. Optical conductivity

From the linear response theory, the optical conductivity is given as

$$\text{Re } \sigma_{\mu\mu'}(\omega) = \sum_{\mathbf{k}\sigma} \int d\epsilon \frac{f(\epsilon) - f(\epsilon + \omega)}{\omega} \times \text{Tr} [\text{Im } G(\mathbf{k}, \epsilon) j_{\mu}(\mathbf{k}) \text{Im } G(\mathbf{k}, \epsilon + \omega) j_{\mu'}(\mathbf{k})] \quad (7)$$

The matrix element of the current operator is defined as

$$j_{\mu}^{mm'}(\mathbf{k}) = -e \frac{\partial h^{mm'}(\mathbf{k})}{\partial k_{\mu}} \quad (\mu = x, y, z). \quad (8)$$

From Eqs.(5) and (7), the optical conductivity is then calculated as

$$\text{Re } \sigma_{\mu\mu'}(\omega) = \int d\epsilon \frac{f(\epsilon) - f(\epsilon + \omega)}{\omega} \times \sum_{\mathbf{k}\sigma} \sum_{\alpha\alpha'} I_{\alpha\alpha'}(\mathbf{k}, \epsilon, \epsilon + \omega) \times \text{Tr} [A_{\alpha}(\mathbf{k}) j_{\mu}(\mathbf{k}) A_{\alpha'}(\mathbf{k}) j_{\mu'}(\mathbf{k})], \quad (9)$$

where $A_{\alpha}(\mathbf{k}) = U(\mathbf{k})E_{\alpha}U^{-1}(\mathbf{k})$, $I_{\alpha\alpha'}(\mathbf{k}, \epsilon_1, \epsilon_2) = D_{\alpha}(\mathbf{k}, \epsilon_1)D_{\alpha'}(\mathbf{k}, \epsilon_2)$, $E_{\alpha}^{mm'} = \delta_{mm'}\delta_{m\alpha}$, and $D_{\alpha}(\mathbf{k}, \omega) = -\frac{1}{\pi} \text{Im } G_{\alpha}(\mathbf{k}, \omega)$. The \mathbf{k} -integration in Eq. (9) should be carefully carried out.

The \mathbf{k} -integration is able to be carried out simply by the generalized tetrahedron method if the integrand has one pole. Since the two-body Green's function $I_{\alpha\alpha'}(\mathbf{k}, \epsilon_1, \epsilon_2)$ has two poles, we should rewrite it to separate into two partial fractions as

$$I_{\alpha\alpha'}(\mathbf{k}, \epsilon_1, \epsilon_2) = \frac{1}{2} \text{Re} [G_{\alpha}(\mathbf{k}, \epsilon_1)G_{\alpha'}^*(\mathbf{k}, \epsilon_2) - G_{\alpha}(\mathbf{k}, \epsilon_1)G_{\alpha'}(\mathbf{k}, \epsilon_2)] = \frac{1}{2} \text{Re} \left(\frac{G_{\alpha}(\mathbf{k}, \epsilon_1) - G_{\alpha'}^*(\mathbf{k}, \epsilon_2)}{G_{\alpha}^{-1}(\mathbf{k}, \epsilon_1) - \{G_{\alpha'}^*(\mathbf{k}, \epsilon_2)\}^{-1}} - \frac{G_{\alpha}(\mathbf{k}, \epsilon_1) - G_{\alpha'}(\mathbf{k}, \epsilon_2)}{G_{\alpha}^{-1}(\mathbf{k}, \epsilon_1) - G_{\alpha'}^{-1}(\mathbf{k}, \epsilon_2)} \right). \quad (10)$$

In case $\alpha = \alpha'$, the denominator of Eq. (10) is actually \mathbf{k} -independent and the generalized tetrahedron method can be applied.

When $\omega \sim 0$, we should treat Eq. (10) separately for $\alpha = \alpha'$ and $\alpha \neq \alpha'$. When $\omega \sim 0$ and $\alpha = \alpha'$, Eq. (10) is then rewritten as

$$I_{\alpha\alpha}(\mathbf{k}, \epsilon, \epsilon) = \frac{1}{2} \text{Re} \left[|G_{\alpha}(\mathbf{k}, \epsilon)|^2 + Z(\epsilon) \frac{\partial G_{\alpha}(\mathbf{k}, \epsilon)}{\partial \epsilon} \right], \quad (11)$$

$$Z(\epsilon) = \left[1 - \frac{\partial \Sigma(\omega)}{\partial \omega} \Big|_{\omega \rightarrow \epsilon} \right]^{-1}. \quad (12)$$

When $\omega \sim 0$ and $\alpha \neq \alpha'$, Eq. (10) should be rewritten as

$$I_{\alpha\alpha'}(\mathbf{k}, \epsilon, \epsilon) = \frac{1}{2} \text{Re} \left\{ [(\epsilon - \text{Re } \Sigma(\epsilon) - \epsilon_{\alpha}(\mathbf{k}))(\epsilon - \text{Re } \Sigma(\epsilon) - \epsilon_{\alpha'}(\mathbf{k})) + (\text{Im } \Sigma(\epsilon))^2 + i(\epsilon_{\alpha}(\mathbf{k}) - \epsilon_{\alpha'}(\mathbf{k})) \text{Im } \Sigma(\epsilon)]^{-1} - \frac{G_{\alpha}(\mathbf{k}, \epsilon)G_{\alpha'}(\mathbf{k}, \epsilon)}{\epsilon_{\alpha}(\mathbf{k}) - \epsilon_{\alpha'}(\mathbf{k})} \right\}. \quad (13)$$

In the above two cases, the resultant $I_{\alpha\alpha'}(\mathbf{k}, \epsilon, \epsilon)$ can be calculated by using the generalized tetrahedron method.

For cases of t_{2g} bands, the \mathbf{k} -dependent Green's function is diagonal and this is also true for $I_{\alpha\alpha'}(\mathbf{k}, \epsilon, \epsilon)$. However, for e_g bands, the \mathbf{k} -dependent Green's function has non-zero off-diagonal elements and also $I_{\alpha\alpha'}(\mathbf{k}, \epsilon, \epsilon)$

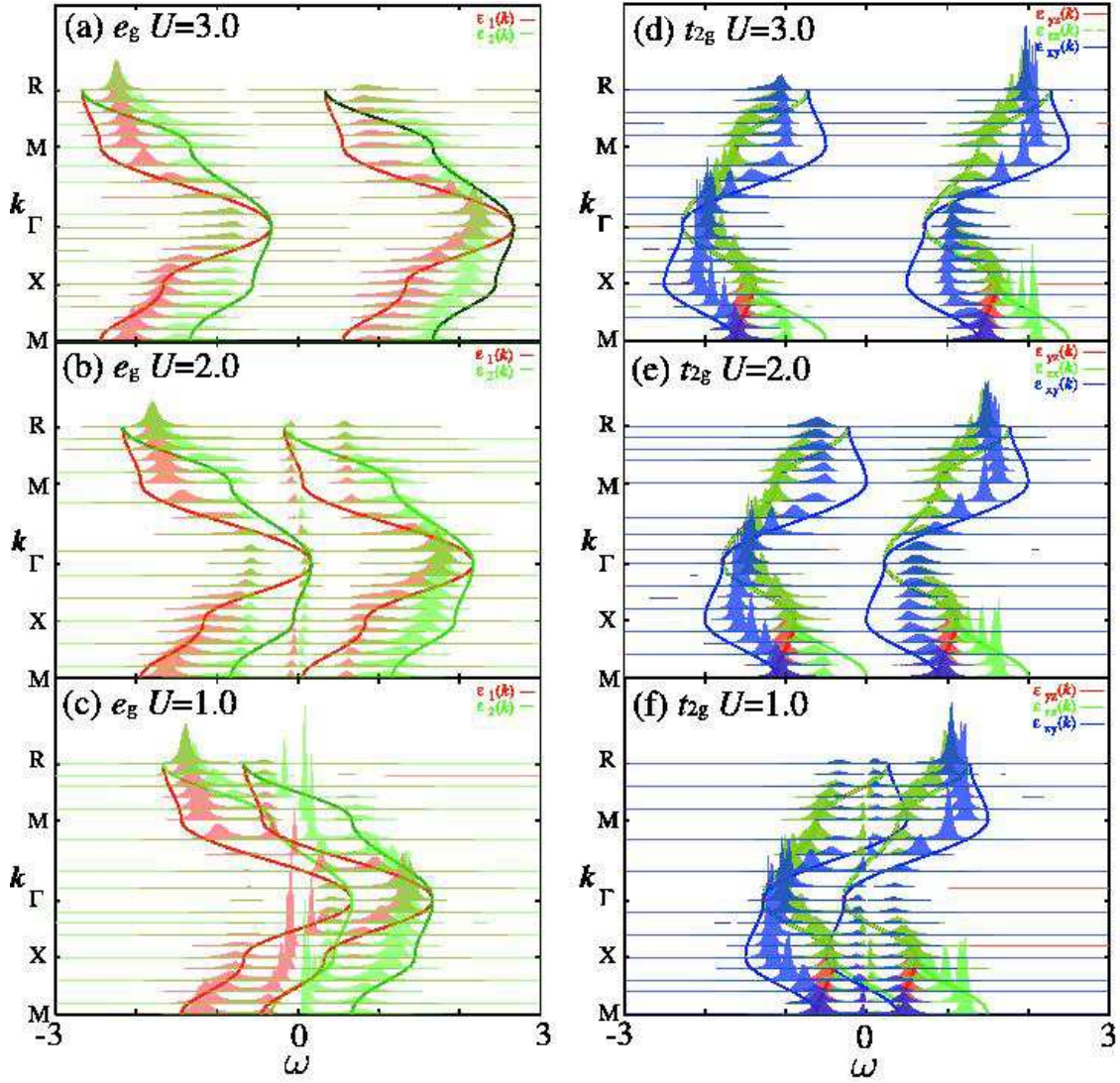


FIG. 1: The imaginary part of the \mathbf{k} -dependent Green's function $G(\mathbf{k}, \omega)$ (shaded regions) of e_g bands and t_{2g} bands on a simple cubic lattice. The energy bands $\epsilon(\mathbf{k})$ shifted by $\pm U/2$ at high-symmetry lines are also shown. The high-symmetry \mathbf{k} -points are $M(\frac{\pi}{2}, \frac{\pi}{2}, 0)$, $X(\frac{\pi}{2}, 0, 0)$, $\Gamma(0, 0, 0)$, $R(\frac{\pi}{2}, \frac{\pi}{2}, \frac{\pi}{2})$. (a) e_g bands, $U = 3.0$. (b) e_g bands, $U = 2.0$. (c) e_g bands, $U = 1.0$. (d) t_{2g} bands, $U = 3.0$. (e) t_{2g} bands, $U = 2.0$. (f) t_{2g} bands, $U = 1.0$. The inverse temperature $\beta = 30$. In the e_g bands cases (a)~(c), red and green shades represent $G_{11}(\mathbf{k}, \omega)$ and $G_{22}(\mathbf{k}, \omega)$ of the diagonalized \mathbf{k} -dependent Green's function matrix, respectively. In the t_{2g} bands cases (d)~(f), red, green and blue shades represent $G_{yz, yz}(\mathbf{k}, \omega)$, $G_{zx, zx}(\mathbf{k}, \omega)$ and $G_{xy, xy}(\mathbf{k}, \omega)$, respectively.

has. Then the denominators of Eq. (10) in case of $\alpha \neq \alpha'$ for e_g bands are \mathbf{k} -dependent and, therefore, \mathbf{k} -integration is not able to be carried out by using the generalized tetrahedron method. For this case, \mathbf{k} -integration should be carried out as the sum of the integrand at each $\omega + i\delta$.

D. The energy bands

We have applied the above described calculation scheme to the doubly degenerate e_g bands ($N_{\text{deg}} = 4$) and the triply degenerate t_{2g} bands ($N_{\text{deg}} = 6$). We consider Slater-Koster-type tight-binding Hamiltonian on a simple cubic lattice. The effective hopping integrals are assumed only between the nearest neighbor pairs and $V_{dd\sigma} = 1/3$, $V_{dd\pi} = -2/3V_{dd\sigma}$ and $V_{dd\delta} = 1/6V_{dd\sigma}$. The relationship among $V_{dd\sigma}$, $V_{dd\pi}$ and $V_{dd\delta}$ is the scaling properties of bare two-center integrals in the LMTO

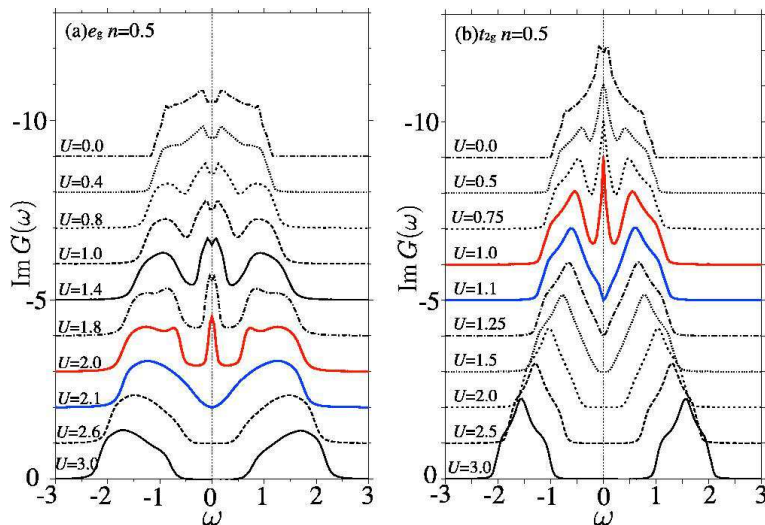


FIG. 2: The imaginary part of the local Green's functions in a half-filled case $n = 0.5$. (a) Doubly degenerate e_g bands of the half band width $D = 7/6$. (b) Triply degenerate t_{2g} bands of the half band width $D = 1$. The inverse temperature $\beta = 30$.

method. Here the half band width of e_g orbitals and t_{2g} orbitals are $D_{e_g} = 3(V_{dd\sigma} + V_{dd\delta}) = 7/6$ and $D_{t_{2g}} = 2(V_{dd\pi} - V_{dd\delta}) = 1$, respectively. The off-diagonal elements of $h(\mathbf{k})$ of arbitrary \mathbf{k} are non zero for the e_g bands. On the other hand, those for the t_{2g} bands are always zero.

III. NUMERICAL RESULTS

A. \mathbf{k} -dependent spectrum

The imaginary part of \mathbf{k} -dependent Green's function $G(\mathbf{k}, \omega)$ is shown in Fig. 1 (shaded regions) with the energy bands $\epsilon(\mathbf{k})$ (full lines), for $\beta = 30$ and the electron occupation $n = 1/2$ (a half-filled case). The energy zeroth is set to be at the chemical potential μ . Energy bands $\epsilon(\mathbf{k})$ are shifted by $\pm U/2$, corresponding to lower and upper Hubbard bands.

Within the Fermi liquid theory, the \mathbf{k} -dependent Green's function behaves as

$$G(\mathbf{k}, \omega) \simeq Z / \{\omega \mathbf{1} - Zh(\mathbf{k})\} \quad (14)$$

near $\omega \sim 0$ in a metallic case, where $Z = (1 - \frac{\partial \Sigma}{\partial \omega})^{-1}$ is a renormalization factor. Then the width of the coherent peak at the Fermi energy is scaled by $1/Z$. These values become constant within the DMFT, since the \mathbf{k} -dependence of the self-energy Σ is \mathbf{k} -independent.

In the e_g band case, peaks appear at the Fermi energy for $U = 1.0$ and $U = 2.0$, which shows that the system is in a metallic phase. For $U = 1.0$, those peaks strongly depend on \mathbf{k} and the spectrum becomes sharper rapidly near the Fermi energy. On the contrary, for $U = 2.0$, those peaks hardly depend on \mathbf{k} . With increasing Coulomb interaction in a metallic phase ($U =$

2.0), coherent peaks appear. At $U = 3.0$, the spectrum splits into upper and lower Hubbard bands. This results from the combination of electronic structure calculation and DMFT. The model calculation of DMFT with only assuming the density of states is not able to give the \mathbf{k} -dependent spectra.

It must be noted that, in t_{2g} case, the spectrum shows already the coherent peak hardly depending upon \mathbf{k} at $U = 1.0$ and it splits into upper and lower Hubbard bands at $U = 2.0$.

B. Imaginary part of the local Green's function

1. $n = 1/2$ case

The imaginary part of the local Green's function $G_{mm\sigma}(\omega)$ is shown in Fig. 2, for $\beta = 30$, with the electron occupation $n = 1/2$ (a half-filled case). The positive and negative energy regions, corresponding to the spectrum of excitation from occupied to unoccupied states (electron ionization spectrum) and that from unoccupied to occupied states (electron affinity spectrum).

In a half-filled case, the spectrum consists of the upper and lower Hubbard bands with the electron-hole symmetry. At the critical region (here, $U \simeq 2.0$ for e_g bands and $U \simeq 1.0$ for t_{2g} bands) one observes a sharp coherent peak at $\omega \simeq 0$. In an insulating case, the self energy shows the singular behavior $\Sigma \sim \frac{1}{\omega}$ near $\omega \sim 0$. On the contrary, In a metallic case, the self energy behaves as $\Sigma - Un(N_{deg} - 1) \sim \omega$ near $\omega \sim 0$, which is typical for the Fermi liquid.

As seen in Fig. 2, the critical U/D ratio is different between e_g bands and t_{2g} bands; $(U/D)_{cr} \simeq 1.71$ for e_g bands and $(U/D)_{cr} \simeq 1.0$ for t_{2g} bands. Figure 2

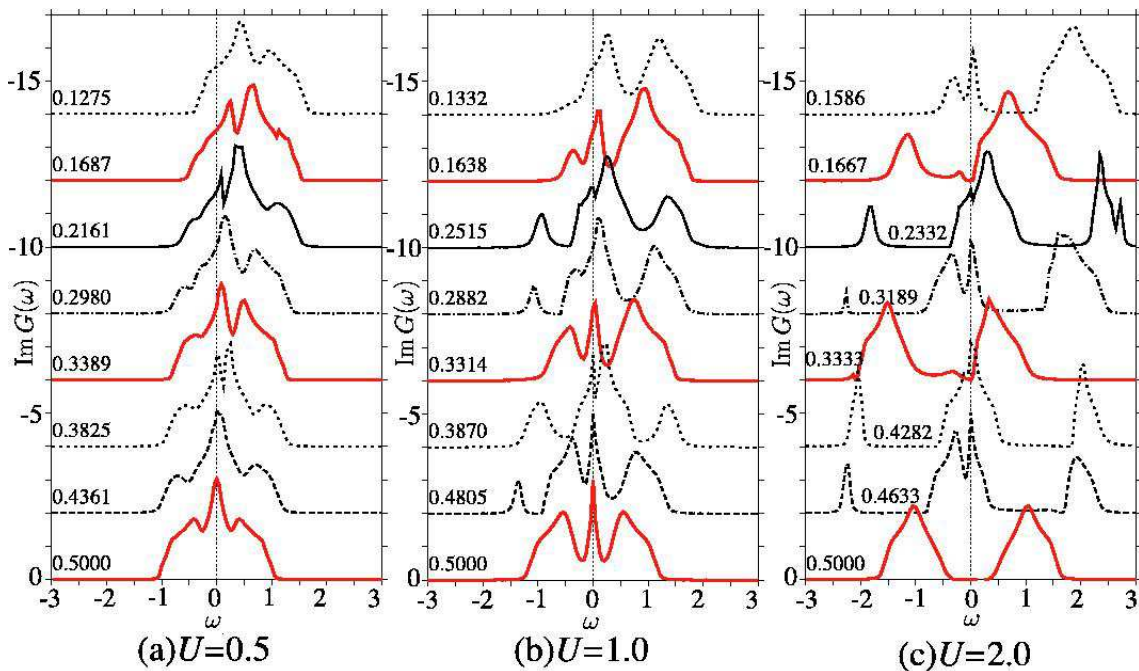


FIG. 3: The electron occupation dependence of the imaginary part of local Green's functions for the triply degenerate t_{2g} bands of the half band width $D = 1$ and the inverse temperature $\beta = 30$. The numbers in the figure denote the electron occupation per each orbital. Red line shows the case of the (almost) integer filling of the total d-electron number $n = 1/6$ ($n_d = 1$), $n = 1/3$ ($n_d = 2$) and $n = 1/2$ ($n_d = 3$).

also shows that in the insulating case, the band width is shrinking more at the same U/D ratio for t_{2g} bands than that is for e_g bands. This is because that the self-energy is much larger for t_{2g} bands than for e_g bands for the same U/D value due to the degree of the degeneracy with respect to spins and orbitals, N_{deg} . The second-order self-energy is proportional to $(N_{deg} - 1)U^2$ and it contributes $5/3$ times larger for t_{2g} bands than for e_g bands. This fact means that the critical U/D ratio of metal-insulator transition decreases with increasing degeneracy, which contradicts to the conventional understandings that the critical U/D ratio would be the same as in the s-orbital case, [15] or that the critical U/D ratio would increase with it. [16] These contradiction could originate from the Hamiltonian on a lattice or the symmetry type of the orbitals.

2. $n < 1/2$ case

Figure 3 shows the electron occupation dependence of the imaginary part of the local Green's functions for t_{2g} bands with $\beta = 30$. (See Ref. 9 for e_g -band.) In case of $n = 1/6$ ($n_d = 1$), $n = 1/3$ ($n_d = 2$) and

$n = 1/2$ ($n_d = 3$), one observes the coherent peak at $\omega \simeq 0$ for $U = 1.0$, which is the critical region of metal-insulator transition. We also observe the gap for the same n 's at $\omega \simeq 0$ for $U = 2.0$ and system becomes insulator. These occupations correspond to the cases of the integer filling of the total d-electron number. At the integer filling case of $n_d = i$ (i :integer), the states of $n_d = i$ is completely filled and the states of $n_d = i + 1$ is completely empty. Then the gap opens between the ionization and affinity spectra.

With small hole doping δ , in which electron occupation $n_d = i - \delta$, the spectrum changes drastically at $U = 1.0$ and $U = 2.0$. Since the ground state is the mixture of the states of $n_d = i$ and $n_d = i - 1$, a sharp peak appears below the lower Hubbard band. This satellite peak corresponds to the electron ionization of $n_d = i \rightarrow i - 1$. The ionization and affinity levels for both $n_d = i$ and $n_d = i - 1$ states appear in the spectrum. These satellite structures of all configurations of $n_d = 0, 1, 2, \dots$ appear but their intensity depends on the occupation number. With increasing hole doping δ , the electron ionization spectrum gradually increases. On the contrary, the electron affinity spectrum loses the intensity. When the occupation approaches $n_d = i - 1$ from

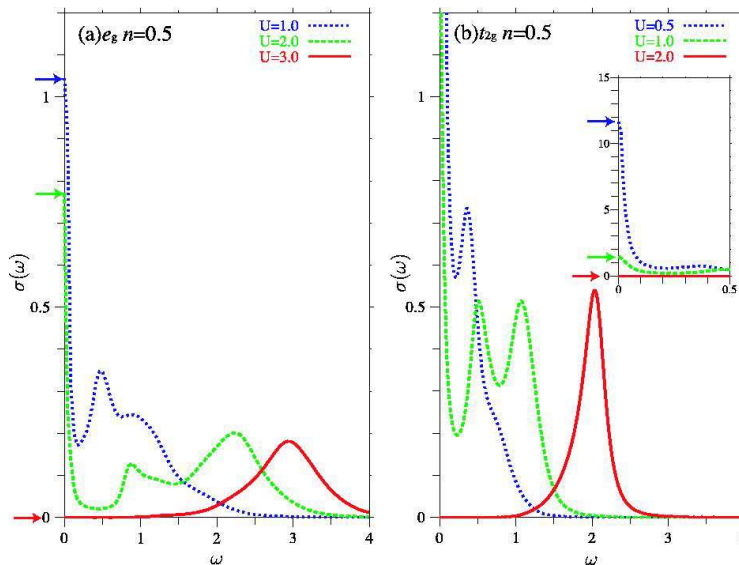


FIG. 4: The optical conductivity in a half-filled case $n = 0.5$. (a) Doubly degenerate e_g bands of the half band width $D = 7/6$. (b) Triply degenerate t_{2g} bands of the half band width $D = 1$. The inverse temperature $\beta = 30$. The arrows indicate the height of the Drude peak.

above, the electron affinity spectrum $n_d = i \rightarrow i + 1$ disappears.

From above discussion, we have had success of the spectrum calculation which simultaneously shows the effects of multiplet structure and DMFT such as the electron ionization and affinity levels of different electron occupations, coherent peaks at the Fermi energy in the metallic phase and a gap at an integer filling of electrons for sufficiently large Coulomb U .

C. Optical conductivity

1. $n = 1/2$ case

Figure 4 shows the optical conductivity in a half-filled case. In a metallic case, ($U = 1.0, 2.0$ for e_g bands, $U = 0.5, 1.0$ for t_{2g} bands) three peaks appear: (1) the Drude peak at $\omega \sim 0$, (2) a peak of the width $2D$ at $\omega < U$ and (3) a peak of the width $4D$ at $\omega = U$. The peak (2) comes from the transition from the coherent state to the upper Hubbard band or that from the lower Hubbard band to the coherent state. The peak (3) at U comes from the transition from the lower Hubbard band to the upper Hubbard band. The peaks (1) and (2) result from the DMFT which includes the coherent state.

With increasing Coulomb U in metallic phase, contributions of the peaks (1) and (2) decreases. In the insulating case, ($U = 3.0$ at e_g bands, $U = 2.0, 3.0$ at t_{2g} bands) the peaks (1) and (2) disappear and only that of (3) remains. Figure 4 is consistent with the fact that the critical U/D ratio is different between e_g bands and t_{2g} bands [$(U/D)_{cr} = 1.71$ for e_g bands and $(U/D)_{cr} = 1.0$

for t_{2g} bands].

2. $n < 1/2$ case

Figures 5 and 6 show the optical conductivity in cases of arbitrary electron occupations. In case of the integer filling of the total d-electron number, such as $n = 1/6$ ($n_d = 1$), $n = 1/3$ ($n_d = 2$) and $n = 1/2$ ($n_d = 3$), for $U = 2.0$, the Drude peak disappears and one observes only a peak at $\omega = U$, which comes from the transition from the lower Hubbard band to the upper Hubbard band.

With small hole doping δ , in which electron occupation $n_d = i - \delta$ (i =an integer number), the Drude peak appears and the peak at $\omega = U$ shrinks. One also observes a peak which is separated from Drude peak at $\omega \sim 0.4$ for both $U = 1.0$ and $U = 2.0$. With increasing hole doping δ , this peak shifts toward lower energy and becomes sharper and merges into the Drude peak, because it comes from the transition from the lower Hubbard band to the coherent state. At this range, the height of the Drude peak becomes higher and sharper. Also we can see that the intensity at the lower energy side of the peak at $\omega = U$ decreases simultaneously, and this is because that this side of the peak at $\omega = U$ were mainly contributed by the transition from the coherent state to the upper Hubbard band. When the occupation approaches $n_d = i - 1$ from the above, the Drude peak disappears again for $U = 2.0$.

Optical conductivity successfully shows the ionization and affinity transition and also metal-insulator transition. This is, of course, consistent with the results of the

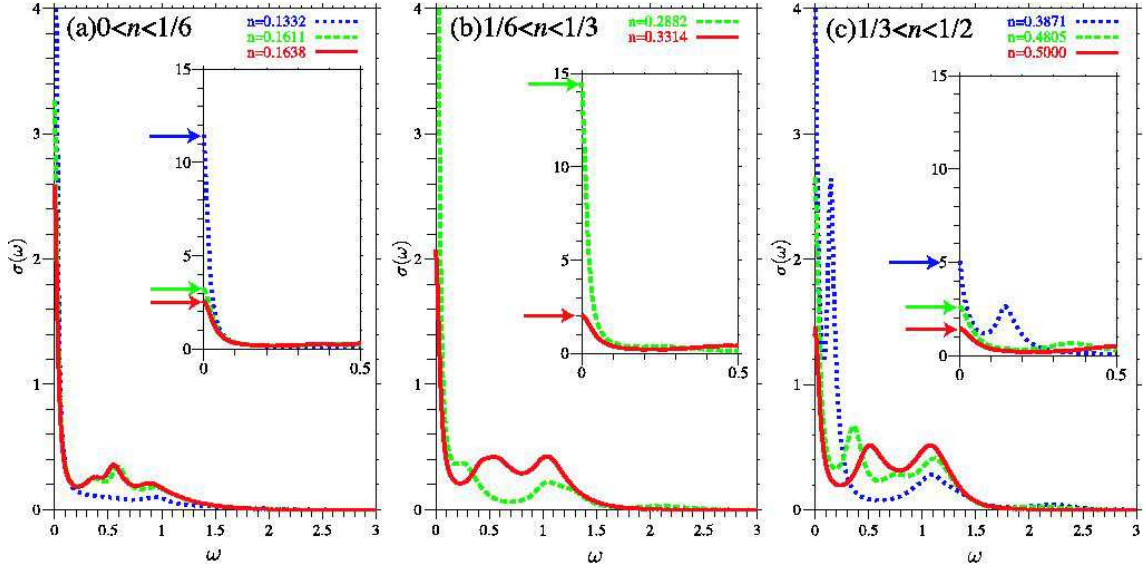


FIG. 5: The electron occupation dependence of the optical conductivity at $U = 1.0$ for the triply degenerate t_{2g} bands of the half band width $D = 1$. The inverse temperature $\beta = 30$. The numbers in the figure denote the electron occupation per each orbital. (a) $0 < n \leq 1/6$ ($0 < n_d \leq 1$), (b) $1/6 < n \leq 1/3$ ($1 < n_d \leq 2$), (c) $1/3 < n \leq 1/2$ ($2 < n_d \leq 3$). The arrows indicate the height of the Drude peak.

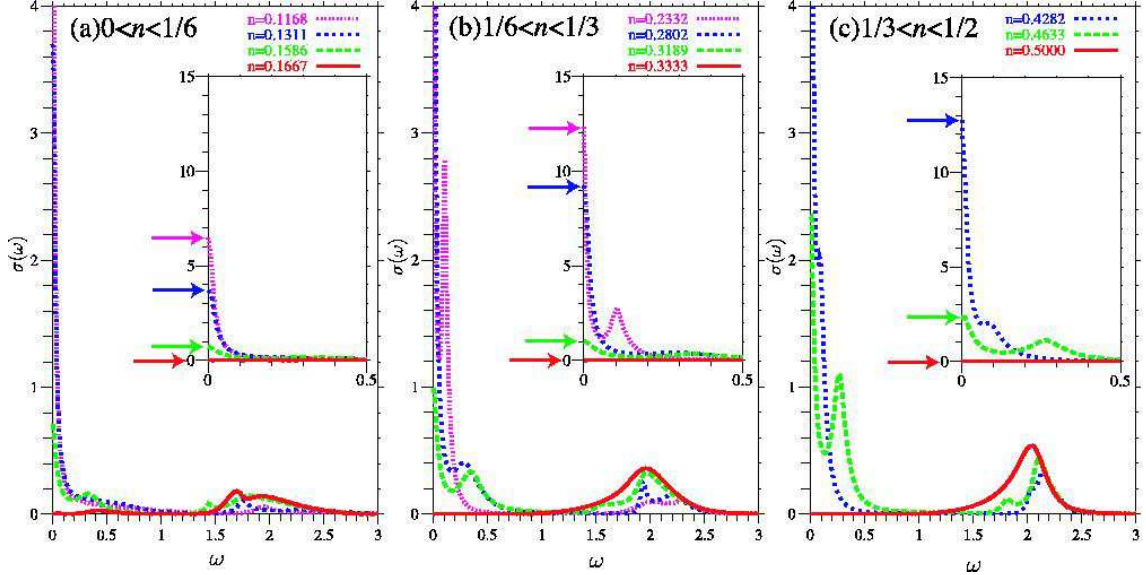


FIG. 6: The electron occupation dependence of the optical conductivity at $U = 2.0$ for the triply degenerate t_{2g} bands of the half band width $D = 1$. The inverse temperature $\beta = 30$. The numbers in the figure denote the electron occupation per each orbital. (a) $0 < n \leq 1/6$ ($0 < n_d \leq 1$), (b) $1/6 < n \leq 1/3$ ($1 < n_d \leq 2$), (c) $1/3 < n \leq 1/2$ ($2 < n_d \leq 3$). The arrows indicate the height of the Drude peak.

spectrum.

IV. CONCLUSION

In conclusion, we have applied the generalized DMFT-IPT method to doubly degenerate e_g bands and triply

degenerate t_{2g} bands. The \mathbf{k} -dependent spectrum shows the resonance behavior near the Fermi energy at smaller U and the coherent peak near metal-insulator transition. The spectrum shows that the critical U/D ratio of metal-insulator transition is different between e_g bands and t_{2g} bands and this originates from the degeneracy N_{deg} . In the arbitrary occupation case, the spec-

trum shows ionization and affinity levels, coherent peaks at the Fermi energy in a metallic phase and a gap at an integer filling of electrons for sufficiently large Coulomb

U . The optical conductivity gives a spectrum consistent with the above discussions.

-
- [1] A.I. Lichtenstein, V.I. Anisimov and J. Zaanen, Phys. Rev. B **52** (1995) R5467.
- [2] A. Georges, G. Kotliar, W. Krauth and M.J. Rozenberg, Rev. Mod. Phys. **68** (1996) 13.
- [3] V.I. Anisimov, A.I. Poteryaev, M.A. Korotin, A.O. Anokhin and G. Kotliar, J. Phys: Condens. Matter **9** (1997) 7539.
- [4] A.I. Lichtenstein and M.I. Katsnelson, Phys. Rev. B **57** (1998) 6884.
- [5] S. Biermann, F. Aryasetiawan and A. Georges Phys. Rev. Lett. **90** (2003) 086402.
- [6] M.J. Rozenberg, X. Y. Zhang and G. Kotliar, Phys. Rev. Lett. **69** (1992) 1236.
- [7] A. Georges and G. Krauth, Phys. Rev. Lett. **69** (1992) 1240.
- [8] H. Kajueter and G. Kotliar, Phys. Rev. Lett. **77** (1996) 131.
- [9] T. Fujiwara, S. Yamamoto and Y. Ishii, J. Phys. Soc. Jpn. **72** (2002) 777.
- [10] Th. Pruschke and N. Grewe, Z. Phys. B **74** (1989) 439.
- [11] A. Georges and G. Krauth, Phys. Rev. B **48** (1993) 7167.
- [12] Y. Kuramoto and H. Kojima, Z. Phys. B **57** (1984) 95.
- [13] J.M. Luttinger and J.C. Ward, Phys. Rev. **118**, (1960) 1417.
- [14] E. Müller-Hartmann, Z. Phys. B-Condens. Matter **76** (1989) 211.
- [15] M.J. Rosenberg, Phys. Rev. B **55** (1997) R4855.
- [16] J.E. Han, M. Jarrell and D.L. Cox, Phys. Rev. B **58** (1998) R4199.